ICES Journal of Marine Science

ICES Journal of Marine Science (2017), 74(8), 2262–2275. doi:10.1093/icesjms/fsx155

Original Article

Exploiting signal processing approaches for broadband echosounders

Andone C. Lavery[1]*, Christopher Bassett[1‡], Gareth L. Lawson[2], and J. Michael Jech[3]

[1]*Department of Applied Ocean Physics and Engineering, Woods Hole Oceanographic Institution, Woods Hole, MA 02543, USA*
[2]*Biology Department, Woods Hole Oceanographic Institution, Woods Hole, MA 02543, USA*
[3]*NOAA Northeast Fisheries Science Center, Woods Hole, MA 02543, USA*

**Corresponding author: tel: +1 508 289 2345; fax: +1 508 457 2194; e-mail: alavery@whoi.edu.*
‡Present address: NOAA Alaska Fisheries Science Center, Seattle, WA 98115, USA.

Lavery, A. C., Bassett, C., Lawson, G. L. and Jech, J.M. Exploiting signal processing approaches for broadband echosounders. – ICES Journal of Marine Science, 74: 2262–2275.

Received 12 August 2016; revised 19 June 2017; accepted 22 June 2017; advance access publication 28 August 2017.

Broadband echosounders, which transmit frequency-modulated pulses, increase the spectral characterization of targets relative to narrowband echosounders, which typically transmit single-frequency pulses, and also increase the range resolution through broadband matched-filter signal processing approaches. However, the increased range resolution does not necessarily lead to improved detection and characterization of targets close to boundaries due to the presence of undesirable signal processing side lobes. The standard approach to mitigating the impact of processing side lobes is to transmit tapered signals, which has the consequence of also reducing spectral information. To address this, different broadband signal processing approaches are explored using data collected in a large tank with both a Kongsberg–Simrad EK80 scientific echosounder with a combination of single- and split-beam transducers with nominal centre frequencies of 18, 38, 70, 120, 200, and 333 kHz, and with a single-beam custom-built echosounder spanning the frequency band from 130 to 195 kHz. It is shown that improved detection and characterization of targets close to boundaries can be achieved by using modified replica signals in the matched filter processing. An additional benefit to using broadband echosounders involves exploiting the frequency dependence of the beam pattern to calibrate single-beam broadband echosounders using an off-axis calibration sphere.

Keywords: broadband acoustic backscattering, matched-filter signal processing, Simrad EK80 echosounder, WBT, wideband.

Introduction

Narrowband echosounders, transmitting single-frequency sinusoidal pulses, also referred to as continuous wave (CW) tones, have been extensively used for fisheries research and studies of zooplankton ecology for over two and a half decades (Holliday *et al.*, 1989; Foote *et al.*, 1991; Andersen, 2001; Korneliussen and Ona, 2002; Wiebe *et al.*, 2002; Fielding *et al.*, 2012; Scoulding *et al.*, 2015). However, there has been a recent emergence of broadband acoustic backscattering systems transmitting frequency modulated (FM) signals, typically linearly-frequency-modulated signals, or chirps, for characterizing fish and other marine organisms (Foote *et al.*, 2005a,b; Stanton *et al.*, 2010, 2012; Lavery *et al.*, 2010). The success of these broadband systems is built upon a long history of laboratory-based and *in situ* broadband measurements (Holliday, 1972; Simmonds and Armstrong, 1990; Stanton *et al.*, 1998; Thompson and Love, 1996; Zakharia *et al.*, 1996; Stanton, 2009; and references there in). Broadband systems allow acoustic backscattering to be measured continuously over a range of frequencies, thereby increasing the amount of information available for spectral characterization of targets, as compared with narrowband techniques, which measure acoustic backscattering at discrete frequencies.

Here, the term "broadband" refers to a system that uses FM transmit signals and hardware capable of transmitting and

receiving over a range of frequencies. A single broadband transducer can typically transmit sound efficiently over an octave bandwidth, where the upper band frequency is twice the lower band frequency. Transducer bandwidth typically increases with frequency. The term "wideband" refers to a system that combines multiple transducers, each with different broadband or narrowband signals and capabilities, to span a range of frequencies larger than can be achieved with a single transducer. Though multi-frequency narrowband echosounders are wideband, the improvements associated to broadband signal processing techniques cannot be achieved from a collection of narrowband signals.

In addition to improved spectral characterization, broadband matched-filter (MF) processing techniques (Turin, 1960), also referred to as compressed pulse processing (Chu and Stanton, 1998; Ehrenberg and Torkelson, 2000; Stanton and Chu, 2008), can improve the temporal, and thus range, resolution. Although the range resolution of narrowband systems, $\Delta r = \frac{c_w \tau}{2}$ (m), where c_w is the sound speed (m/s), is determined by the duration of the transmitted signal, τ (s), the Δr of broadband systems, after MF processing, is independent of τ, and is instead determined by the inverse signal bandwidth, $1/B$. For example, a narrowband signal of duration $\tau = 1.024$ ms has $\Delta r = 76$ cm, while a broadband pulse with a bandwidth of 100 kHz has $\Delta r \sim 0.75$ cm, regardless of τ. Furthermore, the signal-to-noise ratio (SNR) increases in proportion to $B\tau$ as a result of broadband signal processing gains (Ehrenberg and Torkelson, 2000; Stanton and Chu, 2008; and references therein).

Despite the many benefits of broadband approaches, the use of FM transmit signals can increase the complexity of the calibration, processing, and interpretation of the data. Calibration of broadband systems must account for frequency-dependent absorption, transducer response, and beam pattern. Although there is a rich literature on the calibration of narrowband echosounders (e.g. Foote *et al.*, 1987; Demer *et al.*, 2015; and references therein) there has been less published research focused on calibration of broadband echosounders. There are various calibration methods for broadband systems that can be used (Dragonette *et al.*, 1981; Foote, 2006; Atkins *et al.*, 2008; Stanton and Chu, 2008; Eastland and Chu, 2014), including using multiple calibration spheres in the far- or near-field, or a single calibration sphere with processing of the frequency-independent scattering from the front face of the sphere.

A practical approach to broadband calibration, similar to narrowband calibration approaches, uses multiple calibration spheres of different sizes (Foote, 2000, 2006; Lavery *et al.*, 2010) spanning the ka range from ~0.5 to 35, where $k = 2\pi/\lambda$ is the wavenumber of the transmitted sound, λ (m) is the wavelength, and a (m) is the sphere radius. Depending on the sphere size and material properties in relation to the frequency band of interest, the frequency-dependent scattering response may have at least one null due to constructive and destructive interference of the scattered sound (Figure 1). Calibration at frequencies close to these nulls tends not to be accurate, as the target strength (TS; dB re 1 m^2) of the sphere is highly sensitive to small variations in material properties (Foote, 2006, 2007). To avoid these uncertainties, narrowband calibrations are generally performed at frequencies distant from the null locations. By using multiple spheres with different sizes, materials, or both, the nulls will occur at different frequencies, allowing calibration across the entire measurement bandwidth for a broadband system (Foote, 2006; Lavery *et al.*, 2010).

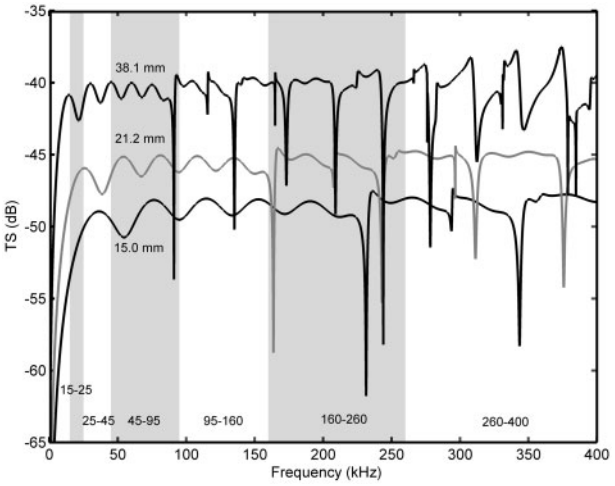

Figure 1. Predicted TS as a function of frequency for spherical tungsten carbide (6% cobalt binder) spheres of three different diameters: 15, 21.2, and 38.1 mm. The predictions are based on the exact modal series solution for an elastic sphere (Faran, 1951). If the scattering responses of the three spheres are plotted as Reduced Target Strength (dB), defined as $RTS = TS - 10\log_{10}(\pi a^2)$, versus ka, then all three curves are identical. The alternating shaded and unshaded regions show the bandwidth of the six Simrad broadband split-beam transducers used in the experiment, with nominal centre frequencies at 18, 38, 70, 120, 200, and 333 kHz.

Though calibration of broadband echosounders is generally more challenging than narrowband echosounders, there are some potential advantages. Most calibrations rely on the position of the calibration sphere in the acoustic beam being known. This may be easily achieved with a split-beam system, in which the transducer is split into four quadrants, allowing the location of a target in the beam to be determined by measuring the phase difference in the signals arriving in each quadrant. However, this can be more challenging with single-beam systems, whether broadband or narrowband. Typical single-beam systems rely on painstakingly maximizing the returns and assuming that the calibration sphere is centered in the beam when the peak return is largest. However, with a broadband system, either single- or split-beam, it is possible to use the frequency dependence of the beam pattern and known spectral response of the sphere to estimate the angle between the sphere and the beam axis. Thus a single-beam broadband echosounder can be calibrated even if the target is not centered in the beam. This approach complements the approach of maximizing the returns to position the target as close as possible to the centre of the beam.

The optimal broadband signals and signal processing approaches for exploiting the increased range resolution of broadband systems for the detection and characterization of targets near boundaries are not well understood. In principle, broadband systems should improve the detection and characterization of targets near boundaries, such as fish near the seabed. These broadband techniques may reduce the volume associated to the acoustic dead zone (Ona and Mitson, 1996; Lawson and Rose, 1999), in the absence of excessive seafloor roughness or slope (Demer *et al.*, 2009; Patel *et al.*, 2009). This could improve acoustic monitoring of some demersal and semi-demersal fish stocks (Hylen *et al.*, 1986; Godø, 1998; Karp and Walters, 1994) and provide information that complements bottom-trawl surveys. However, side lobes resulting from MF processing

may be problematic when the seabed echoes are much stronger than those from nearby fish.

Here, we present results from a series of measurements in a controlled laboratory environment aimed at exploring signal processing techniques to exploit the frequency dependence of the transducer beam pattern to facilitate single-beam broadband calibrations when the position of the target is not known a priori, concurrently achieve full spectral characterization of targets in the free-field and detection and spectral characterization of targets close to boundaries, and evaluate the multiple calibration spheres approach to calibrate an EK80 wideband echosounder across the frequency band from 15 to 400 kHz.

Methods

Two sets of experiments were performed to (i) investigate the use of the frequency-dependent spectrum of a calibration sphere off the central beam axis to locate the sphere in the beam, thus resulting in the possibility of an off-axis calibration for single-beam echosounder, and (ii) better understand the signal processing approaches and limitations for detecting targets close to boundaries. These measurements were performed with a wideband, split-beam, Simrad–Kongsberg (Simrad) EK80 scientific echosounder and with a custom-built echosounder, described in more detail below. Simrad officially released the EK80 broadband scientific echosounder in June 2015. However, the experiments performed here were performed prior to the official release, using earlier versions of the EK80 firmware. The available firmware at the time did not incorporate the built-in calibration function available with the official release; however, all other functionalities were equivalent.

The first experiment, in October 2013, was aimed at calibrating the EK80 in support of field work performed in January 2014 (a companion paper by Jech *et al.*, this issue). These measurements allowed the utility of the frequency-dependent spectrum of a calibration sphere off the central beam axis to locate the sphere in the beam to be investigated.

The second experiment, in April 2015, was aimed at understanding the signal processing approaches and limitations for broadband detection of targets close to boundaries. Approaches to reduce the impact of the processing side lobes were explored, including (i) transmitting different tapered broadband signals, and (ii) implementing a modified MF approach in which the transmit signal is unmodified, but the signal used to perform the MF, also known as the "replica" signal, is strongly tapered. A custom echosounder was also used to explore broadband signals and processing techniques not available in the EK80, such as arbitrary waveforms and a higher sampling frequency of 4 MHz.

Experimental setup

Tank description

All measurements were performed in a large fresh water tank (12-m width, 18-m length, 6-m depth) located in the Jere A. Chase Ocean Engineering facility at the University of New Hampshire, USA (Figure 2). The transducers were aimed horizontally and mounted on a pole connected to an automated, computer-controlled, mobile mounting platform that allowed the depth of the transducer to be set as well as enabling the transducer to be swept angularly through 360° with 0.1° resolution. The platform could be positioned horizontally at any location. Because of limited cable lengths, the distance from the transducers to the wall was slightly different between the EK80 system and the custom echosounder.

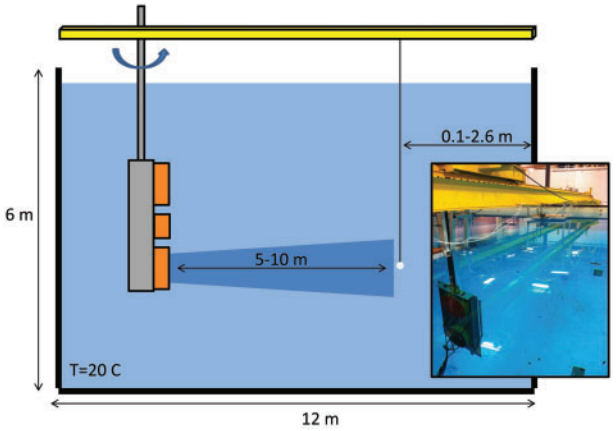

Figure 2. Schematic of the fresh water tank (12 m width, 18 m length, 6 m depth) at the University of New Hampshire. The transducers were pole-mounted and aimed horizontally, with control of the depth, angle, and x-y position in the tank. The inset shows a photograph of the tank and transducer mount.

Description of EK80 scientific echosounder

Calibration measurements for the companion paper by Jech *et al.* (this issue) were obtained using multiple wideband transceivers (WBTs), and multiple Simrad split-beam transducers with nominal centre frequencies, f_{nom}, at 18, 38, 70, 120, 200, and 333 kHz (Table 1) operated by the EK80 software. Each WBT has four channels that can either work independently with a single-beam transducer, or together with a four-quadrant split-beam transducer. The calibration measurements in October 2013 were performed in split-beam configuration. The WBT is designed for applications where power consumption (12–15 VDC, 5 A) and physical size (84 × 213 × 438 mm) are not limiting factors, such as on board a research vessel with GB-Ethernet communications and a data-acquisition computer. The EK80 software controls the WBTs, which can be operated over frequencies ranging from 10 to 500 kHz.

A modified Simrad WBT-Tube system was used for the April 2015 measurements involving calibration spheres close to the tank wall boundary. This system is fundamentally similar to the WBT; however, it has been modified to allow towed operation. All measurements with the WBT-Tube were performed in single-beam configuration. Three depth-rated Simrad transducers were used for these measurements with nominal centre frequencies at 70, 200, and 333 kHz.

The WBTs and WBT-Tube digitized the received signals at 1.5 MHz, which is above the Nyquist sampling criterion for the maximum frequency of 500 kHz. The data from each split-beam transducer were decimated by an amount pre-determined in the EK80 software, which was not user controlled, and was related to the bandwidth of the transmitted signal. There were two stages of decimation and filtering applied in hardware and software in this version of the EK80 echosounder, with a decimation associated with each filter. The filtered and decimated values were saved as complex samples in binary files with a ".raw" extension. All post-processing of EK80 data was performed in MATLAB.

Table 1. Transducer and signal parameters used for the calibration measurements with the Simrad WBTs.

Model	f_{nom} (kHz)	Frequency Range (kHz)	Bandwidth B (kHz)	Full Beam Width	Range Resolution $c_w/2B$ (cm)	*ka* range for WC 15 mm	*ka* range for WC 21.2 mm	*ka* range for WC 38.1 mm
ES18-11	18	15–25	10	11°	7.5	0.48–0.79	0.67–1.12	1.21–2.02
ES38DD	38	25–45	20	7°	3.75	0.79–1.43	1.12–2.02	2.02–3.63
ES70-7C	70	45–95	50	7°	1.5	1.43–3.02	2.02–4.26	3.63–7.66
ES120-7C	120	95–160	65	7°	1.15	3.02–5.08	4.26–7.18	7.66–12.91
ES200-7C	200	160–260	100	7°	0.75	5.08–8.26	7.18–11.67	12.91–20.97
ES333-7C	333	260–400	140	7°	0.54	8.26–12.70	11.67–17.95	20.97–32.26

Other signal configurations and parameters were also tested, but the results presented in this paper are based on the parameters in this table. These parameters were chosen for use in the field work performed in January 2014 as part of a companion study (Jech *et al.*, this issue). With the three WC spheres used, of diameters 15, 21.2, and 38.1 mm, the *ka* range from 0.5 to 33 is entirely spanned with no gaps.

EK80 transmit signals

The EK80 software (version released on 10 October 2013) allowed either linear FM signals, with control of the initial and final frequencies within a system-determined range, or CW signals at the nominal centre frequency of the transducers. The transmitted power and τ were also programmable within system-defined ranges. All results presented here used $\tau = 1.024$ ms. The signals from the different transducers could be transmitted either sequentially or simultaneously. In sequential mode, the transmit interval, which was user programmable, corresponded to the amount of time between the signal transmissions on each transducer. The measurements discussed here were collected either in sequential mode or with only one transducer installed. The "slope," or taper, of the transmitted signal was either "fast" or "slow" (Figure 3a). The fast taper involves smoothly tapering the first two and last two wavelengths with a half cosine wave, equivalent to a Hann window that is not applied to entire signal. The slow taper involves a Hann window applied to the entire signal (Oppenheim and Schafer, 1989). The calibration measurements performed in October 2013 were performed using the fast taper. The measurements of targets close to boundaries with the WBT-Tube in January 2014 were performed with both fast and slow tapers.

Description of the custom echosounder

Data were also collected with a custom echosounder (Lavery and Ross, 2007; Bassett *et al.*, 2015). The transducers used were single-beam (6° full beam width), custom-built, octave-bandwidth transducers (Airmar Technology Corp.) with nominal centre frequency at 160 kHz. The transducers and calibration spheres were set up the same way as for the measurements performed with the EK80 system. The custom echosounder can transmit arbitrary waveforms. The transmit signals used involved 1.024-ms, 130–195 kHz FM pulses. The Airmar transducer frequency band did not fully overlap with the Simrad transducer frequency bands. The 65-kHz bandwidth of the Airmar signal, however, was chosen to be equal to that of the EK80 with the ES120-7C transducer transmitting over the frequency band from 95 to 160 kHz. Two types of tapers were used: (i) an un-tapered FM signal, which resembled the EK80 "fast" taper, and (ii) Gaussian-tapered FM signal with different standard deviations, described below. The transmitted and received signals were sampled at 4 MHz. This high-sampling frequency and

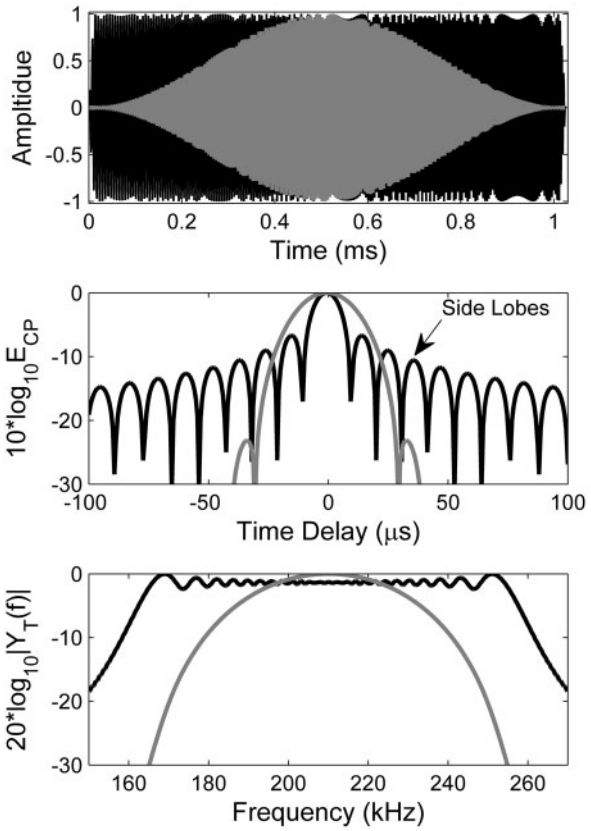

Figure 3. (a) Normalized amplitude for the 200 kHz broadband chirps (160–260 kHz), of 1.024 ms duration, as a function of time for the two EK80 taper options: "fast" taper (black line) and "slow" taper (grey line). (b) $10\log_{10}E_{CP}(t)$ calculated from the autocorrelation of the two signals in (a). The "fast" taper has significant sidelobes compared with the "slow" tapered signal, whereas the main peak of the "fast" tapered signal is significantly narrower than the main peak of the "slow" tapered signal. (c) Spectral amplitude, $20\log_{10}|Y_T(f)|$, of the two signals in (a). The "slow" taper has approximately half the spectral content of the "fast" tapered signal. The ringing and ripples in the spectral response can be clearly seen with the fast taper, known as the Gibbs effect, which is significantly reduced with the slow taper.

the lack of additional filtering and decimation allowed for additional post-processing approaches that are outlined below. The received signals were pre-amplified and saved in binary format as raw voltage versus time, with no decimation applied. All data processing was performed in MATLAB.

Calibration spheres

The calibration measurements involved spheres made from tungsten carbide (WC) with 6% cobalt binder, with diameters of 15, 21.2, and 38.1 mm, commonly used to calibrate narrowband echosounders of similar nominal centre frequencies. Given the frequency bands available and these calibration sphere sizes, *ka* ranged from 0.5 to 33 with no gaps. Calibrations with WC spheres are most reliable with *ka* from ~5 to 16.5, where there are fewer nulls (Lavery *et al.*, 2007, 2010). At higher *ka*, the calibration is more sensitive to rapid changes in the scattering spectrum, target roughness, and knots in the monofilament tether; and at smaller *ka* values, TS is smaller and SNR is lower.

For the WC spheres, the longitudinal sound speed, c_L, used in the *TS* calculations was 6864 m/s, the transverse sound speed, c_T, was 4161 m/s, and the density, ρ, was 14.9 g/cm^3 (Foote and MacLennan, 1984). The tank contained freshwater and the temperature was measured to accurately calculate c_w =1484 m/s (using Fofonoff and Millard, 1983).

Experimental procedure

Procedure for multiple sphere calibration

During the October 2013 measurements, the calibration spheres were suspended using 2-lb test monofilament line, with a diameter of ~ 150 µm, at ranges spanning 5–7 m from the transducers and at a depth of ~2–3 m. The depth of the sphere was controlled to sub-centimetre precision by a motorized pulley system. The height and angle of the transducer under test were adjusted until the target was in the centre of the beam. This was accomplished by maximizing the amplitude of the return from the sphere and by ascertaining that it was located in the centre of the beam according to the split-beam software with no measurable differences in the phases of the signals arriving at the four different split-beam quadrants. For the beam widths and ranges used, the spheres were in the far field of the transducers, conservatively given by a_T^2/λ, where a_T is the transducer radius, and within the first Fresnel zone. Acoustic scattering data were collected with: (i) the spheres located in the centre of the beam at various ranges, and (ii) the transducers rotated so that the sphere moved off the centre of the beam axis in pre-determined angular steps.

Procedure for calibration spheres close to the tank boundary

The single-beam WBT-Tube system was used to measure broadband acoustic backscattering from the WC 38.1 mm sphere located close to the boundary provided by the tank wall. The WC 38.1 mm sphere was chosen for these measurements as it had the highest TS away from the nulls. The WC 38.1 mm sphere was suspended with its centre 10 cm from the tank wall and in the centre of the beam. The target was then moved 10, 20, 30, 50, 75, and 150 cm from the wall. These measurements were performed with the Simrad f_{nom} = 120 kHz channel with both fast and slow tapers. These measurements were then repeated for the custom echosounder for various signal tapers.

Signal processing

Signal processing for on-axis targets

The broadband capabilities of the EK80 echosounder were exploited through the use of MF processing techniques. The received voltage time-series from each of the four split-beam transducer quadrants were filtered, decimated, and saved as complex values by the EK80 data acquisition software. The initial step in the processing involved cross-correlating these received echo-voltage time-series, $v_{R,i}(t)$, on each of the four split-beam quadrants ($i = 1-4$), with the transmitted signal time-series, $v_T(t)$, also referred to as the replica signal. The replica signal time-series was generated at the full sampling frequency (1.5 MHz) and then the same tapers, decimations, and filters were applied as were applied to the received signals. The normalized autocorrelation function of the transmit signal is given by:

$$y_T(t) = \frac{v_T(t) \otimes v_T^*(t)}{|v_T(t)|^2}, \tag{1}$$

where $*$ represents complex conjugate, $||$ represents absolute value, and $\otimes$ represents cross-correlation. The MF output for each of the four split-beam quadrants is given by:

$$y_{R,i}(t) = \frac{v_{R,i}(t) \otimes v_T^*(t)}{|v_T(t)|^2}. \tag{2}$$

When a target is located in the centre of the beam, the averaged pulse-compression signal from all four quadrants is given by $y_R(t)$. The envelope of $y_R(t)$, $E_{CP}(t)$, or its logarithmic form, $10\log_{10}E_{CP}(t)$, is often used to visualize the output of the MF processing (Lavery *et al.*, 2010). However, E_{CP} does not incorporate the calibration measurements, so E_{CP} for different channels cannot be directly compared.

The measured, un-compensated, frequency-dependent, target strength (TS) is given by (modified from Lavery *et al.*, 2010; Stanton *et al.*, 2010; L. Anderson, Simrad, pers. comm.):

$$TS^{\mathrm{meas}}(f) = 10\log_{10}\frac{|Y_R(f)|^2}{|Y_T(f)|^2} - 10\log_{10}L_{TL}(f)^2 - 10\log_{10}(K_T P_T). \tag{3}$$

where f is the acoustic frequency, $|Y_R(f)|$ is the absolute value of the Fourier transform of $y_R(t)$, and $|Y_T(f)|$ is the absolute value of the Fourier transform of $y_T(t)$. The N-point MATLAB fast Fourier transform algorithm was used for these calculations, padded with zeros if the chosen window had fewer than N points (Press *et al.*, 1992). The value of N was chosen to be the next power of 2 larger than the window size in order to optimize the algorithm performance. If a larger power of 2 is chosen, then frequency smoothing results.

The frequency-dependent transmission loss on a linear scale, $L_{TL}(f)$, attributable to spherical spreading and absorption, is $L_{TL}(f) = \frac{10^{-2\alpha(f)r/20}}{r^2}$, where $\alpha(f)$ is the frequency-dependent absorption factor (dB m^{-1}). P_T accounts for the transmit power and is a parameter that can be varied in the EK80 software. K_T is a parameter to correct for the received power of a matched load: $K_T = 2Z\frac{\lambda_{\mathrm{nom}}^2}{16\pi^2}$, where λ_{nom} is the wavelength at the nominal centre frequency and Z accounts for the system hardware impedance (according to the manufacturer $Z \approx 75\ \Omega$). This parameter is

likely a function of frequency, but is not critical to the calculations, as it is accounted for in the system calibration.

The frequency-dependent system calibration for each transducer, $G(f)$, is the difference between the TS^{meas} and the theoretically predicted TS based on the exact modal series solution for a solid elastic sphere, $TS^{\text{model}}(f)$, using the exact size and material properties of the sphere:

$$G(f) = 0.5\left(TS^{\text{meas}}(f) - TS^{\text{model}}(f)\right). \quad (4)$$

The factor 0.5 is retained to be consistent with Simrad's approach for narrowband and broadband systems (Andersen, 2001; Lunde *et al.*, 2013).

Frequency-dependent beam pattern for off-axis targets

For a constant-radius transducer, the transducer beamwidth decreases with increasing frequency. Thus, a target located off-axis is closer to the "edge" (−3 dB points) of the main lobe at higher frequencies than at lower frequencies. A consequence of this is that the measured $TS(f)$ of a target located off-axis (uncorrected for position) appears to decrease with increasing frequency relative to the spectrum of a target located in the centre of the main lobe. It is possible to use this frequency-dependent "droop" in the frequency response of the sphere to infer the angular position of the target in the beam. The one-way beam pattern is given by Medwin and Clay (1998):

$$D_T(f,\ \theta) = \left(2\ \frac{J_1(ka_T\sin\theta)}{ka_T\sin\theta}\right)^2, \quad (5)$$

where $J_1$is the first order cylindrical Bessel function, and θ is the angle. The predicted TS is given by

$$TS^{\text{model, off-axis}}(f,\theta) = TS^{\text{model}}(f) - 10\log_{10}D_T^2(f,\theta). \quad (6)$$

The angular position, θ_{target}, of a target can be determined by comparing the measured $TS(f)$ for an off-axis target, $TS^{\text{meas, off-axis}}\left(f,\theta_{\text{target}}\right)$, to $TS^{\text{model, off-axis}}(f,\theta)$ over a range of values of θ (for example, by calculating least squares differences). It is then possible to also determine the frequency-dependent calibration curve. This analysis was performed for various spheres and frequency bands.

MF processing: side lobes and signal tapers

A less welcome feature associated with MF signal processing is the presence of processing side lobes (Figure 3). When an un-tapered signal is transmitted, the MF processing results in side lobes that emerge from the cross-correlation operation. The side lobes of the MF can be suppressed by tapering the transmitted signal (Figure 3). However, tapering the transmit signal is also associated with a corresponding loss in bandwidth, as well as a loss of range resolution associated with the widening of the main lobe of the MF. The two signal tapering options provided by the EK80, the "fast" and the "slow" tapers, corresponded to transmitting either very slightly tapered chirps, with good spectral bandwidth but high side lobes, or a very strongly tapered signal with less spectral bandwidth and lower side lobes. These two tapers are implemented by using the appropriate "replica" transmit signal in Equation (2), i.e. by replacing $v_T(t)$ with either $v_T^{\text{slow}}(t)$ or $v_T^{\text{fast}}(t)$.

Suppression of processing side lobes can also be accomplished by transmitting an un-tapered signal and then using a tapered "replica" signal to perform the MF in post-processing. This approach was only implemented for the data collected with the custom echosounder. Similar post-processing steps were also applied to the EK80 data but the results are not presented. This is because the stage-2 (software) filter in the EK80 software produced artefacts that could not be suppressed by tapering in post-processing. Future changes to the EK80 software could, in theory, permit similar processing to be applied to EK80 data with comparable results. For the custom echosounder, Gaussian tapers were used to perform this "post-processing" as, theoretically, Gaussian tapered signals have no side lobes (Priestley, 1981). The Gaussian taper can be applied in the frequency or time domain. In the time domain [modified from Equation (8) in Chu and Stanton, 1998], the Gaussian taper is described by

$$GT(t) = e^{-\frac{(t-t_c)^2}{2\sigma_t^2}}, \quad (7)$$

where t_c is the centre of the transmit signal in time and σ_t is the standard deviation, which controls the degree of tapering. For a given bandwidth and signal duration, the larger the time-domain standard deviation (σ_t), the faster the taper and the closer the signal becomes to an un-tapered, or "square" FM pulse. It is also possible to implement the Gaussian taper in the frequency domain, where the frequency-domain taper is a Gaussian shaped function. The frequency- and time-domain standard deviations, for a given signal duration and bandwidth, are related by $\sigma_f = \frac{B}{\tau}\sigma_t^{-1}$. In the time domain, the Gaussian post-processing taper is implemented by replacing $v_T(t)$ in Equation (2) with $v_T^{GT}(t) = GT(t)\cdot v_T(t)$, where $v_T(t)$ is the actual transmitted signal. Thus, Equation (2) becomes:

$$y_{R,i}(t) = v_{R,i}(t) \otimes \frac{v_T^{GT}(t)^*}{\left|v_T^{GT}(t)\right|^2}. \quad (8)$$

Three primary Gaussian tapers were implemented for the custom echosounder: (i) $\sigma_f = 6$ kHz, equivalent to $\sigma_t = 0.095$ ms for a $\tau = 1.024$ ms duration signal, (ii) $\sigma_f = 15$ kHz, equivalent to $\sigma_t = 0.236$ ms for a $\tau = 1.024$ ms duration signal, and (iii) $\sigma_f = 30$ kHz, equivalent to $\sigma_t = 0.472$ ms for a $\tau = 1.024$ ms duration signal.

Results

Calibration curves based on multiple on-axis calibration spheres

The frequency-dependent calibration curves [Equation (4)] using multiple WC spheres of different sizes for the Simrad transducers are shown in Figures 4 and 5. These measurements were performed with the WC 38.1, 21.2, and/or 15.0-mm targets on-axis, as determined by the positioning of the automated tank calibration set-up as well as by the EK80 split-beam processing.

For the 18-, 38-, and 70-kHz channels, the calibration curves are based on the 21.2-mm target (Figure 4a–c, blue curves). A single calibration was used and there was no need for interpolation. It was found that the usable bandwidth was between 16 and

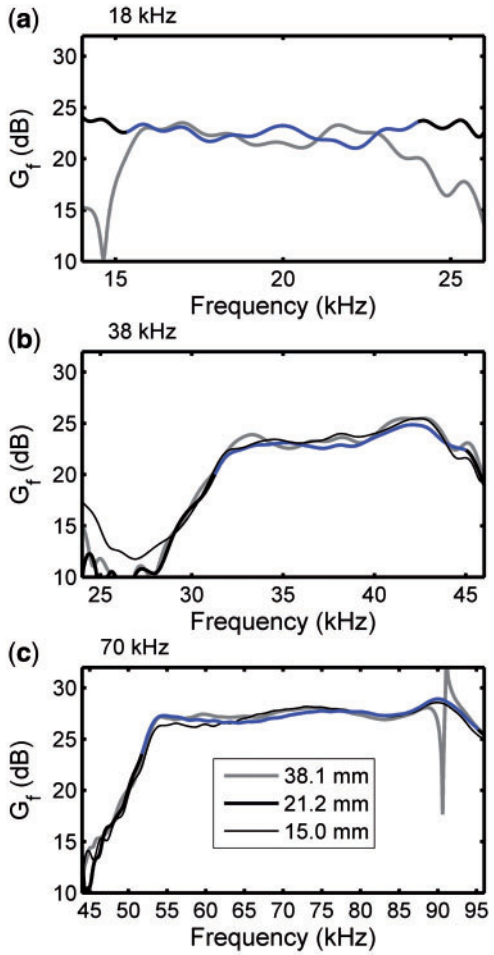

Figure 4. Calibration curves [Equation (4)], $G(f)$ (dB), as a function of frequency based on different calibration spheres, WC 15 mm, WC 21.2 mm, and WC 38.1 mm, for the following Simrad broadband transducers: (a) f_{nom} = 18 kHz with bandwidth from 15 to 25 kHz, (b) f_{nom} = 38 kHz with bandwidth from 25 to 45 kHz, and (c) f_{nom} = 70 kHz with bandwidth from 45 to 95 kHz. Data were not collected with the WC 15 mm calibration sphere with the 18 kHz transducer. The final calibration curves for these three channels are shown in blue and are based entirely on the WC 21.2 mm calibration sphere.

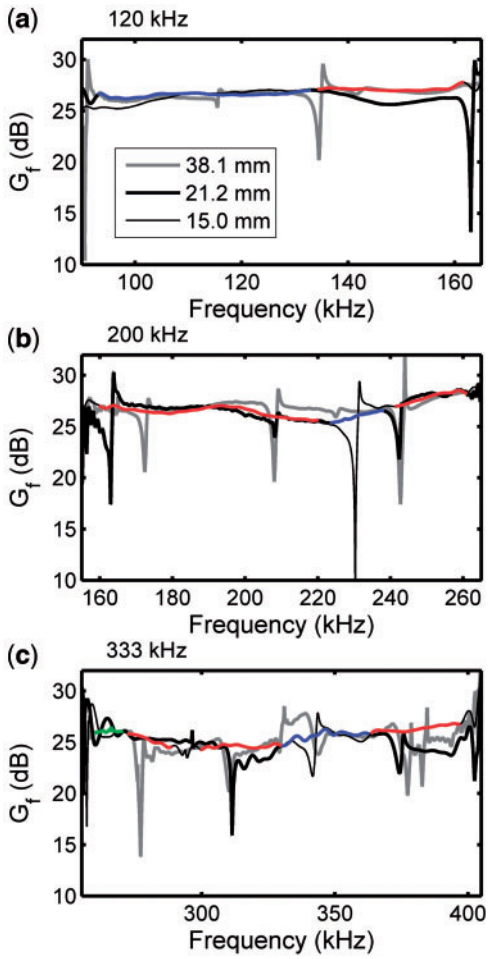

Figure 5. Calibration curves [Equation (4)], $G(f)$ (dB), as a function of frequency based on different calibration spheres, WC 15 mm, WC 21.2 mm, and WC 38.1 mm, for the following Simrad broadband transducers: (a) f_{nom}= 120 kHz with bandwidth from 95 to 160 kHz, (b) f_{nom} = 200 kHz with bandwidth from 160 to 260 kHz, and (c) f_{nom}= 333 kHz with bandwidth from 260 to 400 kHz. The final calibration curves for these channels are based on a combination of calibration spheres: the WC 15 mm calibration sphere is shown in red, the WC 21.2 mm calibration sphere is shown in blue, and the WC38.1 mm calibration sphere is shown in green. Even with these three calibration spheres, it is necessary in interpolate over small frequency bands due to excessive structure in the sphere returns.

24 kHz for the 18-kHz channel, between 31 and 44 kHz for the 38-kHz channel, and between 52 and 95 kHz for the 70-kHz channel (~ -3 dB down points). Though there was some variability between the calibration curves based on the three different calibration spheres, the variability was $<$0.8 dB within the useful bandwidth. This has also been seen previously in the literature (Hobæk and Forland, 2013).

For the 120-kHz channel (Figure 5a), the final calibration curve is based on the combination of the calibration curves for the 21.2-mm target below $\sim$134 kHz (blue line), and the 15-mm target above 134 kHz (red line). No interpolation of the calibration curve was necessary using these two targets as it was possible to completely avoid the nulls without any gaps in frequency. The useful frequency bandwidth spanned 93–161 kHz and the largest difference in the calibration curves, not including the clear differences that occur in the vicinity of the nulls, occurred in the 140–160 kHz band, but was still smaller than 1.3 dB.

For the 200-kHz channel there was significantly more structure that had to be avoided. In principle, it should be possible to use smaller targets to obtain the final calibration curve without excessive interpolation. However, it is not always feasible to perform operational calibrations with numerous spheres. In addition, as the targets get smaller, TS decreases, and the targets become harder to manage, harder to tether, thinner monofilament line must be used to avoid contamination by the knots making up the tether, and the SNR also decreases. Thus it was decided to limit the smallest sphere to 15 mm.

The final calibration curve for the 200-kHz channel (Figure 5b) was based on the 15-mm target for frequencies from $\sim$160 to 220 kHz (red line), the 21.2-mm target up to a frequency of $\sim$238 kHz (blue line), a small gap from 238 to 241 kHz, and

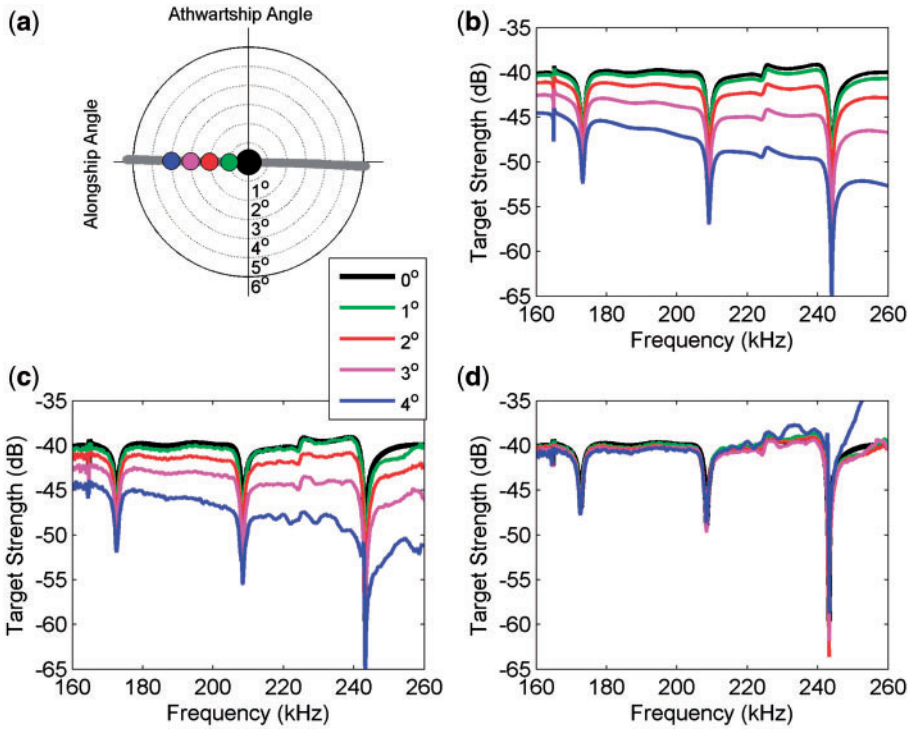

Figure 6. Off-axis calibration: (a) Angular position of the WC 38.1 mm target in the beam as determined by the split-beam processing of the 200 kHz broadband transducer as the transducer is mechanically rotated in 0.1 degree steps through the main beam of the transducer (grey line). Large coloured dots represent the on-axis (black), 1 (green), 2 (red), 3 (pink), and 4 (yellow) degree positions of the target in the beam. (b) Predicted TS as a function of frequency and degrees off-axis. (c) Measured TS as a function of frequency [Equation (3)] for the 200 kHz Simrad broadband channel, when the WC 38.1 mm target is at the angular positions shown by the coloured dots in (a). For the purposes of illustration, the measured TS has been arbitrarily shifted vertically to align with the predicted TS. This vertical offset is accounted for in the final calibration curves [Equation (4)]. (d) Measured TS as a function of frequency for the 200-kHz Simrad broadband channel when the WC 38.1 mm target is at the angular positions shown by the coloured dots in (a) and corrected for the frequency-dependent beam pattern. The off-axis measured TS spectra, shown in (c), collapse onto the on-axis TS spectrum once their angular position in the beam has been accounted for.

finally the 15-mm target up to the upper end of the band at 260 kHz. The small gap between 238 and 241 kHz is a result of excessive structure in all the target responses, and is filled by linear interpolation between the last value of the 21.2-mm target below the gap and the first value of the calibration curve for the 15-mm target above the gap. For the 200-kHz channel, it was only necessary to interpolate 3% of the total bandwidth. This interpolation is reasonable as all three targets show that there was no significant frequency dependent change in the transducer response in this frequency band. The useful frequency bandwidth spanned 160–260 kHz (∼−3 dB points) and the largest difference in the calibration curves, not including the clear differences that occur in the vicinity of the nulls, occurred in the 200–230 kHz band, but was still smaller than 1.2 dB.

As with the 200-kHz channel, there was significantly more structure to be avoided for the 333-kHz channel (Figure 5c). The final calibration curve for the 333-kHz channel was based on the 38.1-mm target for frequencies from 260 to 270 kHz (green line), the 15-mm target for frequencies from 270 to 289 kHz (red line), a gap from 289 to 299 kHz, the 15-mm target for frequencies from 299 to 330 kHz (red line), the 21.2-mm target from 330 to 362 kHz (blue line), and finally the 15-mm target from 262 to 397 kHz (red line). It was necessary to linearly interpolate from 289 to 299 kHz, representing ∼14% of the total bandwidth. The useful frequency bandwidth spanned 260–397 kHz (∼ −3 dB points) and the largest difference in the calibration curves, not including the clear differences that occur in the vicinity of the nulls, occurred in the 380–400 kHz, and was up to 2.5 dB in this high end of the frequency band.

Off-axis calibration

Figure 6a shows the position of the WC 38.1 mm sphere, as determined from the EK80 split-beam processing (grey line), as it was slowly moved horizontally through the 200-kHz transducer beam. Figure 6b shows $TS^{\text{model, off}-\text{axis}}(f, \theta)$ for the WC 38.1 mm target over the frequency band of the 200-kHz transducer for $\theta = 1$, 2, 3, and 4 degrees (corresponding to the locations of the coloured dots in Figure 6a). It is important to note that the position of the nulls does not change. The black curve corresponds to the TS model predictions with the target in the centre of the beam ($\theta = 0$). Figure 6c shows $TS^{\text{meas, off}-\text{axis}}$ for the target at the positions indicated by the coloured dots in Figure 6a, with the black curve corresponding to measurements with the target in the centre of the beam. These TS spectra have not been corrected for the location of the target in the beam; in other words, the processing of the data to arrive at Figure 6c follows the same processing as a target located in the centre of the beam, and the

measured signals on all four split-beam quadrants are averaged together, simulating a single-beam system. Thus, when the target is off-axis, the spectra decrease with increasing frequency. Figure 6d shows the measured TS spectra in Figure 6c corrected for the position of the target in the beam [Equation (6)]. It can be seen that the corrected TS spectra are in close agreement with the spectrum for the target at the centre of the beam. Once the target is sufficiently outside the main lobe (e.g. at $\theta = 4°$), there are larger errors in the corrected TS, particularly at higher frequencies where the beamwidth is narrower. This illustrates that the shape of the spectrum for an off-axis target can be used to determine how far off-axis the target is, though not precisely where in the beam the target is located. For the purposes of calibration, this allows a system to be accurately calibrated even if the target is off-axis by an unknown amount during calibration, so long as it is still within the main beam for some significant portion of the frequency band.

Detection of targets close to boundaries using tapered transmit signals

A comparison of the ability to detect a WC 38.1 mm sphere 30 cm and 1.5 m from the tank wall using an un-tapered transmit signal and a tapered transmit signal is shown in Figure 7. Using the EK80 fast taper for the transmitted signal illustrates that the side lobes associated with the MF signal processing from the tank wall, a strong target, clearly interfere with the detection of a weaker target, in this case the WC 38.1 mm sphere located 30 cm from the boundary (Figure 7a). Similar results were obtained using an un-tapered chirp for the transmitted signal with the custom echosounder (Figure 7b). In fact, without any further post-processing, the WC 38.1 mm target needed to be located further away from the wall than $\sim c_w\tau/2$ for it to be detected with either of these transmit signals. Furthermore, as the distance between the target and the wall decreased, the target was increasingly difficult to identify given that the amplitude of the side lobes from the wall increased but the TS of the sphere did not. For a given taper, if a smaller calibration sphere was used with a smaller TS (Figure 1), the detection range where side lobes were smaller than the amplitude of the sphere increased.

In contrast, when the slow EK80 taper was used for the transmitted signal, it was possible to detect the WC 38.1 mm sphere up to 20 cm separation from the wall (e.g. Figure 7a shows 30 cm separation). When a Gaussian tapered signal ($\sigma_f = 6$ kHz) was transmitted with the custom echosounder, it was possible to detect the WC 38.1 mm sphere up to 10-cm separation from the wall.

Detection of targets close to boundaries using tapered replica signals

A comparison of the MF output from the custom echosounder with the WC 38.1 mm sphere 30 cm from the wall using an un-tapered chirp with the same replica in the MF, a Gaussian tapered chirp with the same replica in the MF, and an un-tapered chirp post-processed with a Gaussian tapered chirp replica in the MF are shown in Figure 8. It was possible to detect the target up to 10-cm range from the boundary while transmitting an un-tapered signal, so long as a strongly tapered signal was used as a replica transmit signal in post-processing. Although the target should be more easily detected close to the boundary using shorter broadband signals (as the side lobes decrease faster with shorter signals, and thus do not extend as far in range), the shorter signal duration comes at the expense of a decrease in the SNR, and in practice no significant improvement in detection was found (data not shown).

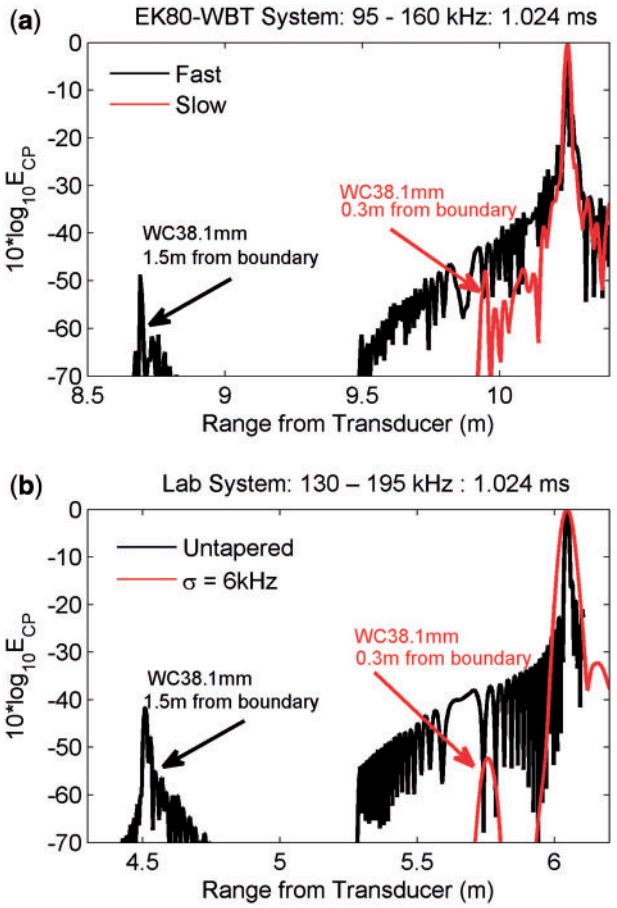

Figure 7. (a) Normalized envelope of the MF output in log space, $10\log_{10}E_{CP}(t)$, for the 120-kHz Simrad transducer transmitting a 1.024 ms duration chirp from 95 to 160 kHz with the "fast" (black line) and "slow" (red line) EK80 taper. The black line corresponds to the WC 38.1 mm sphere located 1.5 m from the boundary (the tank wall). The target can easily be detected as the side lobes from the boundary only extend to $\sim c_w\tau/2$, or 75 cm, from the main return for this signal. The TS is ~40 dB lower than the main peak in the MF output for the boundary. The red line corresponds to the WC 38.1 mm sphere located 0.3 m from the boundary. When the target was located at 0.3 m from the boundary and the signal with the "fast" taper was transmitted, the target could not be detected due to the overlap with the side lobes. However, the target is easily detected when the "slow" taper is transmitted. (b) Same as (a) except these data were collected with the custom echosounder transmitting a 1.024 ms duration chirp from 130 to 195 kHz with no taper and a Gaussian taper with standard deviation of $\sigma_f = 6$ kHz. The separation between the WC38.1 mm target is the same as for the data in (a), however, the total range was smaller due to the different cable lengths.

Spectral characterization of targets close to boundaries

Figures 7, 8a and 8b illustrate that strongly tapering the transmitted signal resulted in improved ability to detect a target in close proximity to a boundary. However, though the target could be

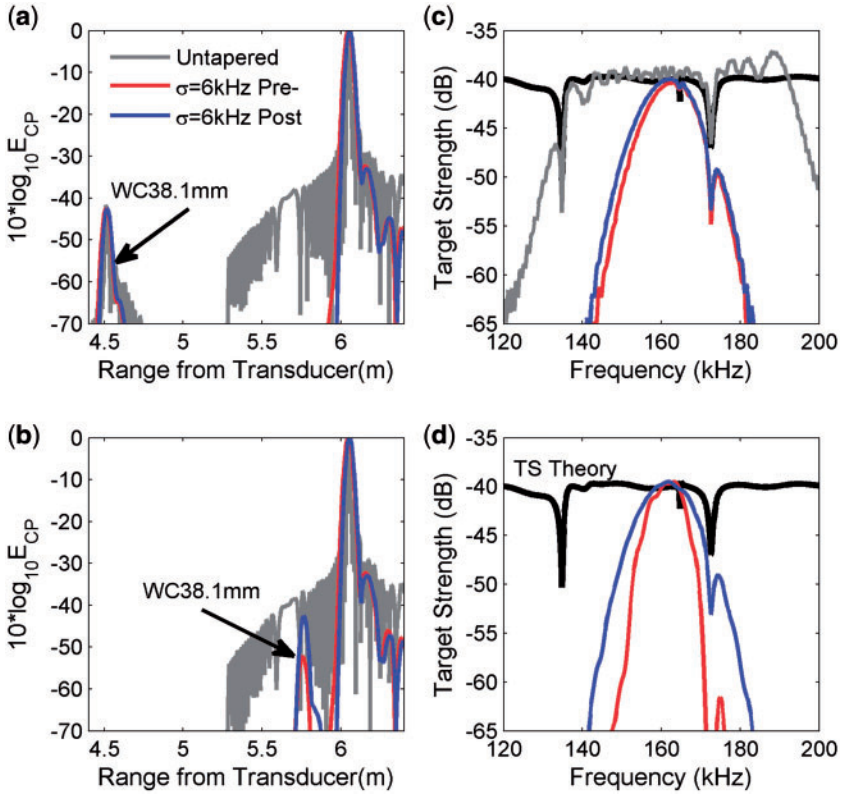

Figure 8. (a, b): Normalized envelope of the MF output in log space, $10\log_{10}E_{CP}(t)$, for the custom echosounder transmitting a 1.024 ms duration chirp from 130 to 195 kHz with no taper (grey line), a Gaussian taper with standard deviation of $\sigma_f = 6$ kHz (blue line), and with no taper but post-processed with a Gaussian taper with standard deviation of $\sigma_f = 6$ kHz (red line). (a) The WC 38.1 mm target is 1.5 m from the boundary (the tank wall), and (b) the WC 38.1 mm target is 0.3 m from the boundary. (c) Measured TS spectrum of the WC 38.1 mm target 1.5 m from the boundary. For the purposes of illustration, the measured spectra have been arbitrarily shifted to match the predicted TS at f_{nom}. (d) Measured TS spectrum of the WC 38.1 mm target 0.3 m from the boundary. For the purposes of illustration, the measured spectra have been arbitrarily shifted to match the predicted TS at f_{nom}. With either the pre- or post-processed signals there is significant loss in the spectral content of the signal, but that the ability to detect the target is similar for either the pre- or post-processed signals. In fact, while the detectability is similar, there is more spectral content with the post-processed signal.

detected to small target-boundary separations, the strongly tapered transmit signals also resulted in a decrease in the effective bandwidth available to spectrally characterize the target (Figure 8c and d). In addition, some of the energy in the side lobe of the boundary echo "leaked" into the signal from the target and resulted in errors in the TS spectra (i.e. differences in measured versus theoretical).

Data collected with the custom echosounder demonstrated that similar characterization of the target was possible when a Gaussian tapered signal was transmitted as when an un-tapered signal was transmitted (Figure 8c and d). However, in order to obtain this same level of detection and characterization when an un-tapering signal was transmitted, it was necessary to post-process the data with a tapered replica signal.

Figure 9 shows a comparison of the un-tapered transmitted chirp and the MF output post-processed using three Gaussian taper widths ($\sigma = 6$, 15, 30 kHz) with the target 30 cm from the tank wall. In all cases, the taper suppresses the side lobes, making the target easily identifiable, at the expense of increased width of the main lobe (associated with loss in spatial resolution). There is a clear loss in spectral information of the target as the taper becomes more aggressive (Figure 9b). This highlights the need to balance target detection with the desire to adequately characterize the target.

Discussion

Measurements of acoustic scattering over a wide frequency band offer the potential for improved target discrimination and characterization relative to traditional narrowband methods, while simultaneously increasing range resolution and improving signal-to-noise. However, there are also calibration and signal processing challenges that need to be addressed to optimize the capabilities of broadband systems. Till recently, the limited availability of commercial broadband echosounders geared towards fisheries acoustics has not required these issues to be addressed as systematically as they have been for narrowband echosounders. The Simrad EK80 wideband, split-beam, scientific echosounder, released in June 2015, is a welcome arrival, which, however, deserves the same careful scrutiny that was afforded to its earlier narrowband counterparts, the EK60 and EK500 (e.g. Jech *et al.*, 2005).

A Simrad EK80, which combined WBTs with split-beam, transducers with nominal centre frequencies of 18, 38, 70, 120, 200, and 333 kHz, was calibrated in a controlled laboratory environment using multiple calibration spheres of different sizes.

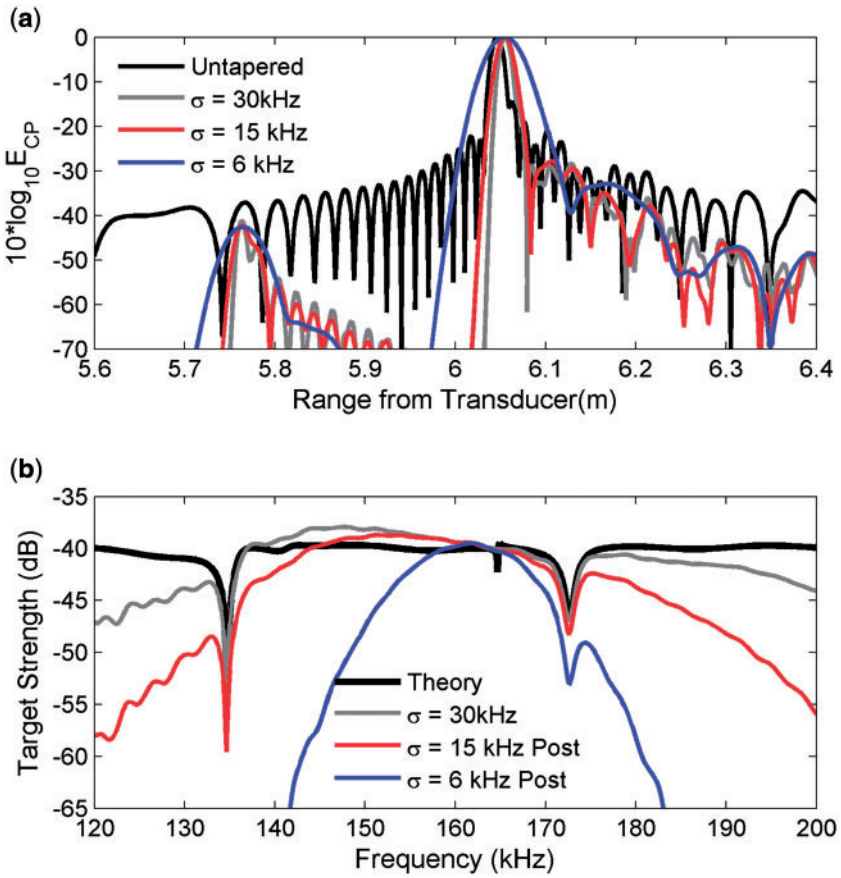

Figure 9. (a) Normalized envelope of the MF output in log space, $10\log_{10}E_{CP}(t)$, for the custom echosounder with the WC 38.1 mm target located 0.3 m away from the boundary and transmitting a 1.024 ms duration un-tapered chirp from 130 to 195 kHz but with post-processing using either no tapering (black line), a Gaussian taper with standard deviation of $\sigma_f = 30$ kHz (grey line), a Gaussian taper with standard deviation of $\sigma_f = 15$ kHz (red line), and a Gaussian taper with standard deviation of $\sigma_f = 6$ kHz (blue line). (b) The measured and scaled TS as a function of frequency for the WC 38.1 mm sphere for the different post-processed signals shown in (a). The black curve in (b) corresponds to the predicted TS as the target could not be detected with an un-tapered signal and no post-processing taper applied. As the taper becomes more aggressive, more frequency bandwidth, and hence spectral information content, is lost, thus reducing the ability to perform characterization as well as detection. Furthermore, as the taper becomes more aggressive, and the effective bandwidth decreases, the width of the main lobe increases, and thus the range resolution decreases.

Though the Simrad EK80 currently markets the 18- and 38-kHz channels as narrowband, this study addressed the possibility of using these transducers in broadband mode. For this study, three tungsten carbide calibration spheres of diameters 15, 21.2, and 38.1 mm were used for the routine calibration. With these spheres, the *ka* range spanned ~0.5–33, resulting in a calibration without the need for excessive (< approximately 15% bandwidth in this study) interpolation across the nulls in the frequency response of the spheres. By using more than one sphere with nulls positioned at different frequencies it was possible to minimize calibration error in the vicinity of the nulls. Three spheres of different sizes were used to provide piecewise calibration coverage across the full band of interest while avoiding nulls, and to ensure that the transducer response did not change rapidly in the frequency band of interest, as it is possible that rapid changes in the vicinity of a null could mask significant changes in the transducer response. Although the general applicability of these three spheres to EK80 broadband calibration in different environments remains to be confirmed, results presented here suggest that the three spheres used here are sufficient for adequate calibration of the EK80 across the available bandwidth. These calibrations have been used in a field study published in a companion paper (Jech *et al.*, this issue).

During this calibration exercise, performed in a large tank with the ability to precisely control the position of the calibration spheres in the beam, the potential to calibrate the EK80 with a broadband single-beam transducer with an off-axis target was investigated. Though the split-beam capabilities of the EK80 make it relatively straightforward to locate the target in the centre of the beam, thus facilitating the calibration of the system, the WBTs and WBT-Tube can be operated in single-beam configuration. One of the advantages of operating the EK80 in single-beam configuration is the increase in the number of broadband channels available. Each split-beam transducer requires four channels to independently digitize the information from each split-beam quadrant. Using each of these channels for a single-beam transducer effectively quadruples the bandwidth of the system, at the expense of target positioning and tracking. Although a split-beam

system is preferable for single target detection and characterization, there are many applications when this is either of no particular advantage (e.g. high density of targets in the sampling volume, particularly a concern at large ranges when the sampling volume is large) or simply not available. Yet it is notoriously challenging to position a sphere in the centre of a single acoustic beam in dynamic calibration environments.

For a narrowband system, the only way to position a sphere in the centre of a single-beam in the field is to carefully move the target to optimize the amplitude of the return. We have shown that an advantage of a broadband system is that it is possible to both optimize the amplitude of the return and determine the angular position of a known calibration sphere by exploiting the strong frequency dependence of the beam width, effectively illustrating that it is not necessary to locate the target in the centre of the beam to calibrate the system. In fact, the latter method may be more effective because the TS spectrum shape is more sensitive than the amplitude of the peak in the MF output to the position of the target in the beam. This calibration approach relies on the spherical symmetry of the sphere and the fact that the position of the nulls in scattering response do not depend on the angular position of the spherical target in the beam. Once the angular position of the sphere in the beam is known, the calibration curve can be determined by correcting for the angular position of the target in the beam. This may be of particular utility in highly dynamic calibration environments where it is not always straightforward to place the sphere reliably in the centre of the beam, and of even higher utility for single-beam systems where there is otherwise no highly effective method for localizing the angular position of the target in the beam, other than using a supplementary split-beam transducer (Wurtzell *et al.* 2016). However, these measurements have been performed in a controlled laboratory environment with high SNR, and the applicability of the methodology in operational conditions still remains to be determined.

Though the increased spectral coverage for improved target classification was the initial motivation that stimulated the development of wideband scientific echosounders, the increased spatial resolution associated to broadband MF signal processing has also triggered substantial excitement within the fisheries community, particularly in light of the potential for increased detection and classification of demersal fish close to the sea floor (Ona and Mitson, 1996; Lawson and Rose, 1999; MacLennan *et al.*, 2004).

A less welcome feature associated with MF techniques is the presence of processing side lobes. The location of these side lobes is dependent on the duration of the transmit signal. When discrete targets are of comparable amplitude and relatively closely spaced (more closely spaced than the transmit signal but further apart than the broadband range resolution determined by the bandwidth), the processing side lobes may overlap but generally have only a limited impact on target detection and/or characterization. On the other hand, when a relatively weak target is located near a strong target or boundary (e.g. demersal fish near the sea floor), the side lobes from the stronger target can entirely mask the presence of the weaker target. As the spatial extent of the side lobes is determined by the signal duration, for a weak target close to a strong boundary, the range at which a weak target can be detected is not significantly better than the detection range of a narrowband system, with the precise improvement depending on SNR and TS.

There are a number of options for side lobe suppression for applications in which the goal is the detection and/or characterization of a target near a boundary. These options include tapering the transmitted signal, transmitting an un-tapered signal or weakly tapered signal and applying a taper signal in post-processing, or transmitting a sufficiently short narrowband CW pulse. This latter option does not involve MF processing and so there are no complications involving side-lobe masking of the target, but also does not allow spectral characterization of the target: It simply represents an option that can improve range resolution. There are benefits and disadvantages to each of these approaches that must be weighed for particular applications.

The first, and most straightforward, option for side lobe suppression is to transmit a tapered chirp, thus reducing the need for additional processing steps. To date, for the EK80, the options for pre-tapered signals are restricted to the "slow" taper option. Limitations associated with transmitting a tapered transmit signal are that some frequency content available for target characterization is lost and the range resolution and SNR decrease. The loss of frequency content can be particularly important if the SNR is low and the tapered portions of the signal are under the noise floor. Furthermore, the frequency content, and associated information, lost by transmitting a tapered signal cannot be recovered, which means that tapered transmit signals also reduce the ability to characterize the frequency response of targets located away from boundaries (e.g. fish up in the water column).

It is also possible to transmit an un-tapered signal and post-process the data using a tapered signal as a replica in the cross-correlations to identify and characterize targets located near boundaries while retaining full spectral coverage of targets far (i.e. more than the pulse duration) from the boundary. The primary benefit of this post-processing approach is that no information is permanently lost. It is possible to process the data in the water column (far from the boundary) using the traditional approach with the un-tapered replica signal and resulting in full spectral coverage for the detection and classification of targets in the water column, with little adverse effects from the side lobes of the MF. The data close to the boundary (closer than the broadband pulse duration) can be independently post-processed using the tapered replica signal, which reduces the adverse effects of the processing side lobes and thus results in improved detection in situations where there is a boundary (or strong target) in the vicinity of a weak target. This technique has been shown to be effective in the laboratory, however, how well this approach works in operational scenarios still remains to be determined.

Finally, the range resolution for detection purposes can also be improved by transmitting a short, narrowband CW signal. For high-frequency transducers (e.g., $f > 70$ kHz), relatively short ($\tau < 100$ μs) CW signals are required to improve upon the range resolution of tapered broadband chirps. However, by transmitting a short, narrowband, CW signal, significant frequency content is sacrificed. Thus detection may be achieved, but there is limited information for the basis of characterization, including for targets far from the boundary. Furthermore, even when applying a taper, MF processing results in higher SNRs. Therefore, even aggressively tapered broadband signals have benefits over CW signals.

Summary

This study demonstrated that the calibration of the EK80 wideband, split-beam scientific echosounder across the full range of available Simrad transducers, including the 18 and 38 kHz transducers, is possible using three WC calibration spheres.

Recommendations for the best *ka* range to perform the calibrations, and which calibration spheres to use for each frequency band are given. It has been shown that, at least in the laboratory, the EK80 can be calibrated in split-beam or single-beam mode, without the need for the calibration sphere to be located in the centre of the beam (and without a priori knowledge of the location of the target in the beam) as the locations of the nulls do not depend on the location of the target in the beam. Finally, signal processing approaches have been explored that identify the signals and parameters that can improve the detection and classification of targets close to boundaries, without sacrificing spectral content for the classification of targets in the water column far from the boundary. Although the current version of the EK80 does not provide full control of some of these parameters, the ability to detect targets close to boundaries with the EK80 is significantly improved through the use of the "slow" tapered transmit signal. Additional flexibility in determining the exact shape of the transmit signal, as well as more control over the signal decimation, could lead to even better system performance.

Acknowledgements

The authors gratefully acknowledge Tom Weber for kindly allowing the acoustic scattering measurements to be performed at the Jere A. Chase Ocean Engineering Facility at the University of New Hampshire, and to Carlo Lanzoni for technical support during the measurements. The authors benefited from many informative discussions with Dezhang Chu, at Northwest Fisheries Science Centre, and the authors would also like to thank Simrad for allowing the authors to test the newly developed EK80 and loaning multiple WBTs for use on this project. The thoughtful and consistent support of Lars Nonboe Andersen is particularly noted. MATLAB code developed for post-processing of the broadband acoustic data will be made available upon request.

Funding

This research was supported by the NOAA Office of Science and Technology, Advanced Sampling Technology Working Group. G.L.L. was partially supported by NOAA Cooperative Agreements NA09OAR4320129 and NA14OAR4320158 through the NOAA Fisheries Quantitative Ecology and Socieconomics Training (QUEST) program. A.C.L. was partially supported through the Office of Naval Research Ocean Acoustics Program.

References

Andersen, L. N. 2001. The new Simrad EK60 scientific echosounder system. Journal of the Acoustical Society of America, 109: 2336.

Atkins, P., Francis, D. T., and Foote, K. G. 2008. Calibration of broadband sonars using multiple standard targets. Journal of the Acoustical Society of America, 123: 3436. Also Proceedings of the Ninth European Conference on Underwater Acoustics, 1, pp. 261–266. Ed. by M. E. Zakharia, D. Cassereau, and F. Luppe. French Acoustical Society, Paris.

Bassett, C., Lavery, A. C., Maksym, T., and Wilkinson, J. P. 2015. Laboratory measurements of high-frequency, acoustic broadband backscattering from sea ice and crude oil. Journal of the Acoustical Society of America, 137: EL32–EL38.

Chu, D., and Stanton, T. K. 1998. Application of pulse compression techniques to broadband acoustic scattering by live individual zooplankton. Journal of the Acoustical Society of America, 104: 39–55.

Demer, D. A., Cutter, G. R., Renfree, J. S., and Butler, J. L. 2009. A statistical-spectral method for echo classification. ICES Journal of Marine Science: Journal du Conseil, 66: 1081–1090.

Demer, D. A., Berger, L., Bernasconi, M., Bethke, E., Boswell, K., Chu, D., Domokos, R. et al. 2015. Calibration of acoustic instruments. ICES Cooperative Research Report No. 326, 136. p.

Dragonette, L. R., Numrich, S. K., and Frank, L. J. 1981. Calibration technique for acoustic scattering measurements. Journal of the Acoustical Society of America, 69: 1186–1189.

Eastland, G., and Chu, D. 2014. Calibration of a broadband acoustic system in near-field. Journal of the Acoustical Society of America, 135: 2176–2176.

Ehrenberg, J. E., and Torkelson, T. C. 2000. FM slide (chirp) signals: a technique for significantly improving the signal-to-noise performance in hydroacoustic assessment systems. Fisheries Research, 47: 193–199.

Faran, J. J. 1951. Sound scattering by solid cylinders and spheres. Journal of the Acoustical Society of America, 23: 405–418.

Fielding, S., Watkins, J. L., Collins, M. A., Enderlein, P., and Venables, H. J. 2012. Acoustic determination of the distribution of fish and krill across the Scotia Sea in spring 2006, summer 2008 and autumn 2009. Deep-Sea Research II, 59-60: 173–188.

Fofonoff, N. P., and Millard Jr, R. C. 1983. Algorithms for Computation of Fundamental Properties of Seawater. Endorsed by Unesco/SCOR/ICES/IAPSO Joint Panel on Oceanographic Tables and Standards and SCOR Working Group 51. Unesco Technical Papers in Marine Science, No. 44.

Foote, K. G. 2000. Standard-target calibration of broadband sonars. Journal of the Acoustical Society of America, 108: 2484–2484.

Foote, K. G. 2006. Optimizing two targets for calibrating a broadband multibeam sonar. *In* OCEANS 2006, pp. 1–4. IEEE, 2006.

Foote, K. G. 2007. Acoustic robustness of two standard spheres for calibrating a broadband multibeam sonar. *In OCEANS 2007-Europe* (pp. 1–4). IEEE, 2007.

Foote, K. G., Atkins, P. R., Francis, D. T. I., and Knutsen, T. 2005b. Measuring echo spectra of marine organisms over a wide bandwidth. In Proceedings of the International Conference on Underwater Acoustic Measurements: Technologies and Results, II, Heraklion, Greece, 28 June–1 July 2005, pp. 501–508. Ed. By J. S. Papadakis, and L. Bjørnø. Institute of Applied and Computational Mathematics (IACM) at the Foundation for Research and Technology (FORTH), Hellas.

Foote, K. G., Chu, D., Hammar, T. R., Baldwin, K. C., Mayer, L. A., Hufnagle, Jr, L. C., ., and Jech, J. M. 2005a. Protocols for calibrating multibeam sonar. Journal of the Acoustical Society of America, 117: 2013–2027.

Foote, K. G., Knudsen, H. P., Korneliussen, R. J., Nordbø, P. E., and Røang, K. 1991. Postprocessing system for echo sounder data. Journal of the Acoustical Society of America, 90: 37–47.

Foote, K. G., Knudsen, H. P., Vestnes, G., MacLennan, D. N., and Simmonds, E. J. 1987. Calibration of acoustic instruments for fish-density estimation: a practical guide. ICES Cooperative Research Report, No. 144. 63 p.

Foote, K. G., and MacLennan, D. N. 1984. Comparison of copper and tungsten carbide spheres. Journal of the Acoustical Society of America, 75: 612–616.

Godø, O. R. 1998. What can technology offer the future fisheries scientist- possibilities for obtaining better estimates of stock abundance by direct observations. Journal of Northwest Atlantic Fishery Science, 23: 105–132.

Hobæk, H., and Forland, T. N. 2013. Characterization of target spheres for broad-band calibration of acoustic systems. Acta Acustica United with Acustica, 99: 465–476.

Hylen, A., Nakken, O., and., and Sunnanå, K. 1986. The use of acoustic and bottom trawl surveys in the assessment of North-East Arctic cod and haddock stocks. A workshop on comparative biology assessment, and management of gadoids from the North

Pacific and Atlantic Oceans. Northeast and Alaska Fisheries Science Centre, Seattle, USA. 1986.

Holliday, D. V., Pieper, R. E., and Kleppel, G. S. 1989. Determination of zooplankton size and distribution with multifrequency acoustic technology. ICES Journal of Marine Science, 46: 52–61.

Holliday, D. V. 1972. Resonance structure in echoes from schooled pelagic fish. Journal of the Acoustical Society of America, 51: 1322–1332.

Jech, J. M., Foote, K. G., Chu, D., and Hufnagle, L. C. Jr., 2005. Comparing two 38-kHz scientific echosounders. ICES Journal of Marine Science, 62: 1168–1179.

Jech, J. M., Lawson, G. L., and Lavery, A. C. Wideband acoustic volume backscattering (15-260 kHz) of Northern krill (*Meganyctiphanes norvegica*) and butterfish (*Peprilus triacanthus*). ICES Journal of Marine Science, 74: 2249–2261.

Karp, W. A., and Walters, G. E. 1994. Survey assessment of semi-pelagic gadoids: the example of walleye pollock, Theragra chalcogramma, in the eastern Bering Sea. Marine Fisheries Review, 56: 8–22.

Korneliussen, R. J., and Ona, E. 2002. An operational system for processing and visualizing multi-frequency acoustic data. ICES Journal of Marine Science, 59: 293–313.

Lunde, P., Pedersen, A. O., Korneliussen, R. J., Tichy, F. E., and Ness, H. 2013. Power-Budget and Echo-Integrator equations for Fish Abundance Estimation, Fisken og Havet no 10/2013, Institute of Marine Research, Bergen, Norway, 39 p.

Lavery, A. C., and Ross, T. 2007. Acoustic scattering from double-diffusive microstructure. Journal of the Acoustical Society of America, 122: 1449–1462.

Lavery, A. C., Chu, D., and Moum, J. N. 2010. Measurements of acoustic scattering from zooplankton and oceanic microstructure using a broadband echosounder. ICES Journal of Marine Science, 67: 379–394.

Lawson, G. C., and Rose, G. A. 1999. The importance of detectability to acoustic surveys of semi-demersal fish. ICES Journal of Marine Science, 56: 370–380.

Medwin, H., and Clay, C. S. 1998. Fundamentals of Acoustical Oceanography. Academic Press, Boston, MA, USA. ISBN-13: 978-0124875708.

MacLennan, D. N., Copland, P. J., Armstrong, E., and Simmonds, E. J. 2004. Experiments on the discrimination of fish and seabed echoes. ICES Journal of Marine Science, 61: 201–210.

Ona, E., and Mitson, R. B. 1996. Acoustic sampling and signal processing near the seabed: the deadzone revisited. ICES Journal of Marine Science, 53: 677–690.

Oppenheim, A. V., and Schafer, R. W. 1989. Discrete-Time Signal Processing. Englewood Cliffs, NJ, USA, pp. 447–448.

Patel, R., Pedersen, G., and Ona, E. 2009. Inferring the acoustic dead-zone volume by split-beam echo sounder with narrow-beam transducer on a nonintertial platform. Journal of the Acoustical Society of America, 125: 698–705.

Press, W. H., Teukolsky, S. A., Vetterling, W. T., and Flannery, B. P. 1992. Numerical Recipes in C: The Art of Scientific Computing, Ch. 12, 2nd edn. Cambridge University Press, Cambridge, UK.

Priestley, M. B. 1981. Spectral Analysis and Time Series. Academic Press, London, UK. ISBN-13: 978 0125649223.

Scoulding, B., Chu, D., Ona, E., and Fernandes, P. G. 2015. Target strengths of two abundant mesopelagics fish species. Journal of the Acoustical Society of America, 137: 989–1000.

Simmonds, E. J., and Armstrong, F. 1990. A wideband echo sounder: measurements on cod, saithe and herring, and mackerel from 27 to 54 kHz. Rapports et Proces-verbaux des Réunions. Conseil International pour l'Éxploration de la Mer, 189: 381–387.

Stanton, T. K., Chu, D., Wiebe, P. H., Martin, L., and Eastwood, R. L. 1998. Sound scattering by several zooplankton groups I: Experimental determination of dominant scattering mechanisms. Journal of the Acoustical Society of America, 103: 225–235.

Stanton, T. K., and Chu, D. 2008. Calibration of broadband active acoustic systems using a single standard spherical target. Journal of the Acoustical Society of America, 124: 128–136.

Stanton, T. K. 2009. Broadband acoustic sensing of the ocean. Journal of the Marine Acoustic Society of Japan, 36: 95–107.

Stanton, T. K., Chu, D., Jech, J. M., and Irish, J. D. 2010. New broadband methods for resonance classification and high-resolution imagery of fish with swimbladders using a modified commercial broadband echosounder. ICES Journal of Marine Science, 67: 365–378.

Stanton, T. K., Sellers, C., and Jech, J. 2012. Resonance classification of mixed assemblages of fish with swimbladders using a modified commercial broadband acoustic echosounder at 1–6 kHz. Canadian Journal of Fisheries and Aquatic Sciences, 69: 854–868.

Thompson, C. H., and Love, R. H. 1996. Determination of fish size distributions and areal densities using broadband low-frequency measurements. ICES Journal of Marine Science, 53: 197–201.

Turin, G. L. 1960. An introduction to matched filters. Institute of Radio Engineers Transactions on Information Theory, IT, 6: 311–329.

Wiebe, P. H., Stanton, T. K., Greene, C. H., Benfield, M. C., Sosik, H. M., Austin, T. C., Warren, J. D., and Hammar, T. 2002. BIOMAPER-II: an integrated instrument platform for coupled biological and physical measurements in coastal and oceanic regimes. IEEE Journal of Oceanic Engineering, 27: 700–716.

Wurtzell, K. V., Baukus, A., Brown, C., Jech, J. M., Pershing, A., and Sherwood, G. D. 2016. Industry-based acoustic survey of Atlantic herring distribution and spawning dynamics in coastal Maine waters. Fisheries Research, 178: 71–81.

Zakharia, M. E., Megand, F., Hetroit, F., and Diner, N. 1996. Wideband sounder for fish species identification at sea. ICES Journal of Marine Science, 53: 203–208.

Handling editor: David Demer